nanomaterials

MDPI

Article

Electromagnetic Interference Shielding of 2D Transition Metal Carbide (MXene)/Metal Ion Composites

Xuefeng Xia and Quanlan Xiao *

International Collaborative Laboratory of 2D Materials for Optoelectronics Science and Technology of Ministry of Education, Institute of Microscale Optoelectronics, Shenzhen University, Shenzhen 518060, China; xiaxuefeng2018@email.szu.edu.cn

* Correspondence: xiaoql@szu.edu.cn

Abstract: In this work, Ti_3C_2, which has a loosely packed accordion-like structure in transition metal carbide (MXene) form, is fabricated and adsorbed by three metal ions ($Fe^{3+}/Co^{2+}/Ni^{2+}$). The electromagnetic interference (EMI) shielding performance of Ti_3C_2 and Ti_3C_2:$Fe^{3+}/Co^{2+}/Ni^{2+}$ films is researched in detail, demonstrating that the EMI shielding effectiveness can be improved by adsorbing by $Fe^{3+}/Co^{2+}/Ni^{2+}$ ions because the metal ion adsorbing can improve the absorption efficiency via electromagnetic wave scattering. The studied Ti_3C_2:$Fe^{3+}/Co^{2+}/Ni^{2+}$ films can be used as good EMI shielding materials for communications, electronics, military, and other applications.

Keywords: MXene Ti_3C_2; electromagnetic interference; $Fe^{3+}/Co^{2+}/Ni^{2+}$

Citation: Xia, X.; Xiao, Q. Electromagnetic Interference Shielding of 2D Transition Metal Carbide (MXene)/Metal Ion Composites. *Nanomaterials* **2021**, *11*, 2929. https://doi.org/10.3390/nano11112929

Academic Editors: Francesc Viñes Solana and Weichun Huang

Received: 17 September 2021
Accepted: 28 October 2021
Published: 1 November 2021

1. Introduction

In recent years, due to the continuous development of science and technology, newer and faster wireless communication networks have been further covering the entire world, and the shrinking of the volume of intelligent electronic devices throughout the world has attracted the attention of people in the field of electromagnetic interference shielding. Because electromagnetic radiation not only causes harm to the human body but also affects the normal use of electronic equipment, and the traditional electromagnetic interference shielding material has difficulty coping with the increasingly sophisticated and miniaturized electronic equipment, the search for new electromagnetic interference shielding materials has become a focus [1–9]. Many articles have studied the electromagnetic shielding effectiveness of some composite materials [10–19]. For example, Bhawal P. et al. [11]. used different mass fractions of CNFs to improve the electromagnetic shielding effectiveness. Ling J. et al. [13]. studied microcellular polyetherimide/graphene composite foams as heat-resistant electromagnetic shielding materials. Li N. et al. [15]. studied single-walled carbon nanotube (SWNT)-polymer composites as excellent lightweight electromagnetic shielding materials. Compared with these polymer materials, research on the electromagnetic shielding effectiveness of two-dimensional materials is limited. Therefore, we use three different ion solutions with the same concentration to study the electromagnetic shielding effectiveness of MXene films doped with different ions. An MXene is a two-dimensional material obtained by chemically etching the A layer of an MAX phase material [20–25]. The M in the MAX phase generally represents an early transition metal, A represents a group XIII or XIV element, and X represents C or N [26–33]. An MXene has low density and high flexibility compared with traditional electromagnetic interference shielding materials and can be well applied in some delicate and tiny environments.

Because an MXene can exhibit a loose-layered structure that causes multiple internal reflections of electromagnetic waves, electromagnetic waves can be dissipated as thermal energy in the material, which contributes greatly to electromagnetic interference shielding [34–40]. In addition, metal is the originally used filler of electromagnetic interference shielding materials. It has excellent electrical conductivity. Metal ions inherit this property,

and their dispersion in polymers is good and does not affect the original mechanical properties of the material [41]. For example, Li^+ ions and K^+ have been used as intercalants to improve the conductivity of two-dimensional materials [42]. Regarding the surface modification of Ti_3C_2, some metal ions enhance the internal scattering, further enhancing the shielding effectiveness for electromagnetic interference. This method also does not increase the volume or quantity of the shielding material, and the shielding effect can be well improved by embedding a small amount [43–46].

Herein, we used this method to obtain Ti_3C_2 with an accordion-like structure by etching Ti_3AlC_2 with hydrofluoric acid (HF). Ti_3C_2/metal ion composite materials were obtained by reacting Ti_3C_2 with $Fe^{3+}/Co^{2+}/Ni^{2+}$ ion solutions, and Ti_3C_2 and Ti_3C_2:$Fe^{3+}/Co^{2+}/Ni^{2+}$ films were obtained by vacuum filtration. Finally, the electromagnetic interference shielding performance of the four films at frequencies of 8–18 GHz was tested by the coaxial method. The results show that the electromagnetic interference (EMI) shielding effectiveness can be improved to different degrees when Ti_3C_2 is adsorbed by $Fe^{3+}/Co^{2+}/Ni^{2+}$ ions, and the most obvious effect is observed for Ti_3C_2 adsorbing by Fe^{3+} ions. This is due to the fact that metal ions adsorption can enhance the conductivity of the materials and improve the absorption effectiveness via electromagnetic wave scattering in the materials. Such EMI shielding materials have a variety of potential applications, such as in communications, electronics, and the military.

2. Methods

2.1. Material Synthesis

The starting materials were Ti_3AlC_2 (99.5%, Mingshan New Materials, Guangzhou, China), hydrofluoric acid (HF, 40 wt%, Macklin, Shanghai, China), ethanol (C_2H_5OH, 99.5%, Hushi, Shenzhen, China), isopropanol (C_3H_8O, 99.5%, Macklin, Shanghai, China), $Fe(NO_3)_3/Co(NO_3)_2/Ni(NO_3)_2$ (Homemade), and deionized water (DI, Homemade).

2.1.1. Preparation of Ti_3C_2 Powder

In this paper, Ti_3C_2 was obtained by selective etching of Ti_3AlC_2 using HF. First, 0.2 g of Ti_3AlC_2 powder was slowly added to 40–50 mL of HF solution in a centrifuge tube in a fume hood (to prevent violent reaction), which were well mixed at a constant temperature of 40 °C and 300 rpm (to prevent liquid splash), and they were fully reacted for approximately 20 h. Then, the mixture was rinsed with deionized water several times until the pH became neutral and dried at 60 °C for 5–8 h in a vacuum oven to obtain pure Ti_3C_2 powder.

2.1.2. Incorporation of Metal Ions

A total of 0.1 g of Ti_3C_2 powder was mixed with 10^{-5} mol·L^{-1} $Fe(NO_3)_3/Co(NO_3)_2/Ni(NO_3)_2$ solutions, and the mixture was sonicated in a water bath for 6 min and stirred at 800 rpm for 3 h. Then, it was centrifuged at 13,000 rpm for 10 min, and the precipitate was collected, washed with DI water several times, and dried at 60 °C for 3 h in a vacuum oven to obtain Ti_3C_2:$Fe^{3+}/Co^{2+}/Ni^{2+}$ powders; the schematic diagram of preparation is shown in Figure 1.

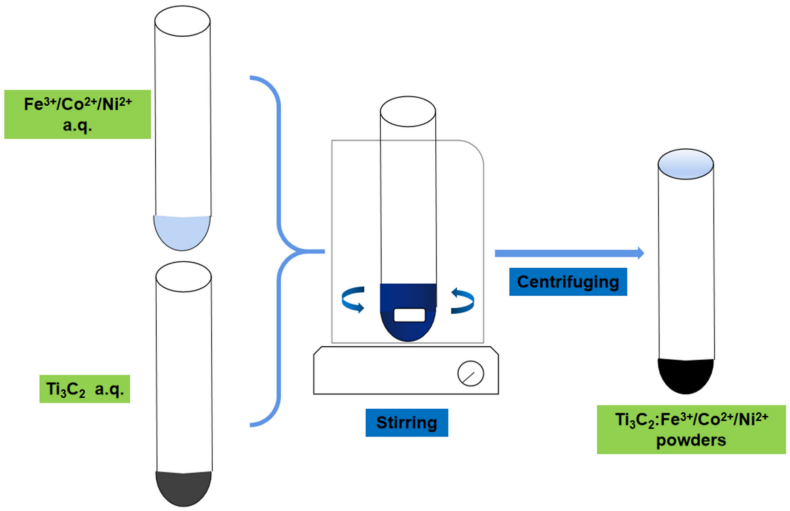

Figure 1. The schematic diagram for the preparation of Ti_3C_2:Fe^{3+}/Co^{2+}/Ni^{2+} powders.

2.1.3. Preparation of Ti_3C_2 and Ti_3C_2:Fe^{3+}/Co^{2+}/Ni^{2+} Films

We used a 20 mL Ti_3C_2 aqueous solution with a concentration of 5 mg/mL and a filter membrane made of Nylon-66 to fabricate a Ti_3C_2 film with a uniform surface by vacuum suction filtration. Similarly, the Ti_3C_2:Fe^{3+}/Co^{2+}/Ni^{2+} films could be obtained using the same method.

2.2. Characterization Methods

We used X-ray diffraction (XRD, Bruker-D8 Advance, Jena, Germany) with Cu/Ka (λ = 0.1541 nm) radiation to investigate the crystal structure and phase purity of the powders. We used a scanning electron microscope (SEM, ZEISS-SUPRA55, Berlin, Germany) and a transmission electron microscope (TEM, JEOL-JEM-3200FS, Tokyo, Japan) to observe the morphology, structure, and size distribution of the powders. We studied the composition of the powders by using the SEM equipped with an energy-dispersive X-ray spectrometer (EDS). A high-resolution transmission electron microscope (HR-TEM) and selected area electron diffraction (SAED) patterns were used to further determine the structure and phase of the powders using the JEOL-JEM-3200FS TEM. The Raman spectra were measured with a Raman spectrometer (Renishaw inVia, Gloucestershire, UK), using a 532 nm laser as the excitation source. The thicknesses of Ti_3C_2, Ti_3C_2/Fe^{3+}/Co^{2+}/Ni^{2+} films were measured using a micrometer (103–137, Mitutoyo, Tokyo, Japan). The electrical conductivity was measured with a conductivity meter (S230-K, Mettler Toledo, Berne, Switzerland). For testing of the electromagnetic interference shielding effectiveness (EMI SE), we used the near-field test method. The instruments used were a spectrum analyzer (FSV40, R&S), a signal source (SMB100A, R&S), and a near-field probe (langer XF1set, Langer emv-technik, Berlin, Germany). First, the signal source frequency and strength were set for the empty window test. Then, the prepared Ti_3C_2 film sample was attached to the sample holder, and the test was started after fixing it. In the same way, Ti_3C_2 films doped with the three different metal ions were tested in sequence. All measurements were performed at room temperature.

3. Results and Discussion

Figure 2a,b shows SEM images of layered Ti_3C_2 after HF treatment. A large number of accordion-like structures of layered Ti_3C_2 can be successfully synthesized by etching with HF, and gaps can be observed among the layers of layered Ti_3C_2 in Figure 2b. It can be inferred that the Al atoms in the original MAX phase have been substantially removed. Figure 2c shows a TEM image of layered Ti_3C_2. The interlayer distance is determined to be 9.86 Å, which is consistent with the previous theoretical value of 9.93 Å [47]. Figure 2d shows an HR-TEM image of layered Ti_3C_2. Parallel and ordered lattice fringes can be

observed in the HR-TEM image, revealing the hexagonal symmetric lattice of layered Ti_3C_2, which matches the results of previous papers [48]. The *d*-spacing of layered Ti_3C_2 is 0.25 nm. Furthermore, the SAED pattern of layered Ti_3C_2 shown in the inset in Figure 2d further reveals the single crystal characteristic of layered Ti_3C_2.

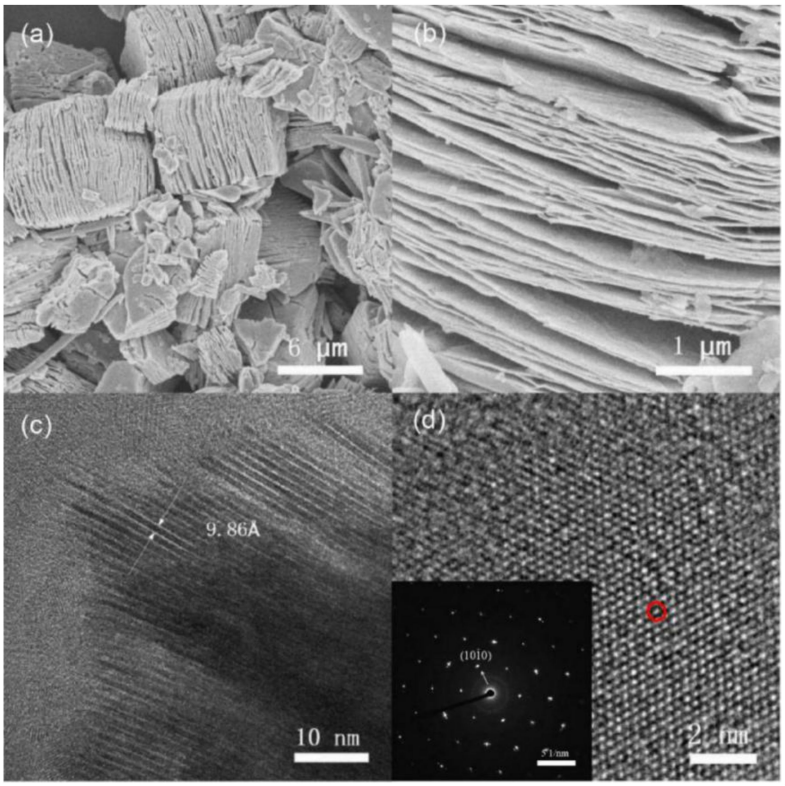

Figure 2. (**a**,**b**) SEM images of layered Ti_3C_2 after HF treatment. (**c**) The interlayer distance of layered Ti_3C_2 sheets was determined via TEM. (**d**) HR-TEM image of Ti_3C_2 and inset showing the corresponding SAED pattern.

Figure 3 shows SEM and EDS mapping images of Ti_3C_2:Fe^{3+}/Co^{2+}/Ni^{2+}. In Figure 3a, we can observe that a large number of nanoparticles appear on the interlayer surfaces of Ti_3C_2:Fe^{3+}. The EDS mapping images of Fe, Ti, and C are depicted in Figure 3b–d, respectively, which are used to investigate the introduction and distribution of Fe^{3+} ions. Similarly, in Figure 3e–l, we can also observe similar phenomena, and a large number of Co^{2+} and Ni^{2+} ions are introduced into layered Ti_3C_2. Therefore, after the reaction of Ti_3C_2 and $Fe(NO_3)_3$/$Co(NO_3)_2$/$Ni(NO_3)_2$ solutions, an obvious adsorbing effect occurs, that is, most of the Fe^{3+}/Co^{2+}/Ni^{2+} ions are distributed on the surface of Ti_3C_2, and the others are intercalated into the layers.

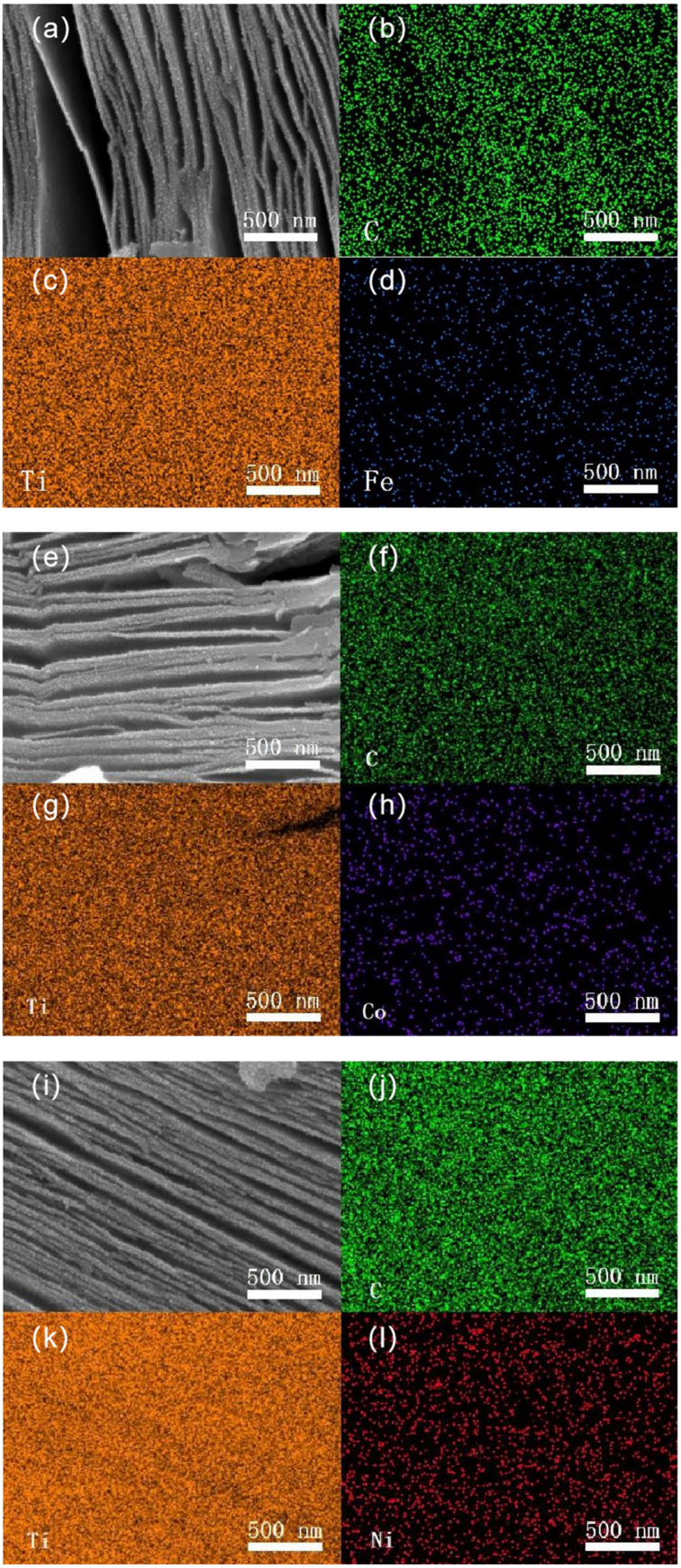

Figure 3. SEM and corresponding EDS mapping images of $Ti_3C_2/Fe^{3+}/Co^{2+}/Ni^{2+}$:$Ti_3C_2/Fe^{3+}$ (**a**–**d**), Ti_3C_2/Co^{2+} (**e**–**h**), and Ti_3C_2/Ni^{2+} (**i**–**l**).

Figure 4 shows the XRD patterns of Ti_3AlC_2, Ti_3C_2, and $Ti_3C_2/Fe^{3+}/Co^{2+}/Ni^{2+}$ powders. Compared with the XRD pattern of Ti_3AlC_2, the prominent peak at ~39° (the (104) plane) disappears completely after etching with HF, which is due to the removal of Al [20–25]. In addition, the peak at ~9° can be attributed to the diffraction of the (002) plane, which has a significant blue shift. According to the XRD data, after Ti_3AlC_2 is etched, the diffraction peak attributed to the (002) plane undergoes a large blue shift (from 9.77° to 9.06°). Ti_3C_2 adsorbed by $Fe^{3+}/Co^{2+}/Ni^{2+}$ has different blue shifts (from 9.06° to 8.82°/8.67°/8.76°), and the intensity of the peak increases upon adsorbing by different metal ions. The main reason for this result should be interpreted as the distribution of the different adsorbing ions in the interlayer space of Ti_3C_2.

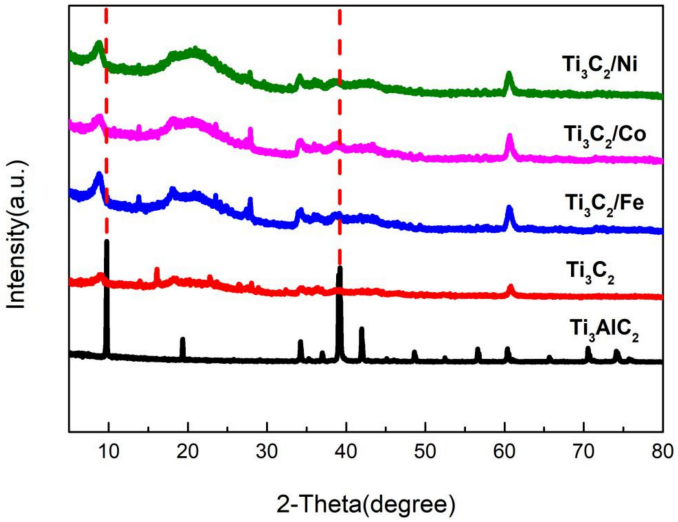

Figure 4. XRD patterns of Ti_3AlC_2, Ti_3C_2, and $Ti_3C_2/Fe^{3+}/Co^{2+}/Ni^{2+}$ powders.

Figure 5 shows the Raman spectra of Ti_3AlC_2, Ti_3C_2, and $Ti_3C_2/Fe^{3+}/Co^{2+}/Ni^{2+}$ powders. In the Raman spectrum of Ti_3AlC_2, two peaks are observed at 280 cm^{-1} and 420 cm^{-1}, both of which are derived from the vibration mode of the Al atom. In the Raman spectrum of Ti_3C_2, these two peaks have disappeared, demonstrating that the Al atom was completely removed after HF etching. In addition, the peak (ω1) at 155 cm^{-1} is enhanced to different degrees when $Fe^{3+}/Co^{2+}/Ni^{2+}$ ions are adsorbed into Ti_3C_2, and the peak can be observed more clearly. It is indicated that the in-plane motion of Ti2 and C atoms may be enhanced by adsorbing metal ions. The peaks (ω2 and ω3) corresponding to out-of-plane stretching vibrations of Ti2 and C atoms appear at 228 cm^{-1} and 599 cm^{-1}, respectively, according to the previous literature [38–46], while the two peaks we obtained appear at 206 cm^{-1} and 617 cm^{-1}, respectively, which indicates that it is possible that the ion adsorption weakened the out-of-plane motion of Ti2 and enhanced the out-of-plane motion of the C atom. According to the Raman spectra, there is no new peak in Ti_3C_2 doped with metal ions, and we can confirm that no new covalent bond vibration modes are generated. Moreover, combined with SEM (Figure 3), we can prove that the metal ions have been tightly bound to Ti_3C_2 by physical adsorption.

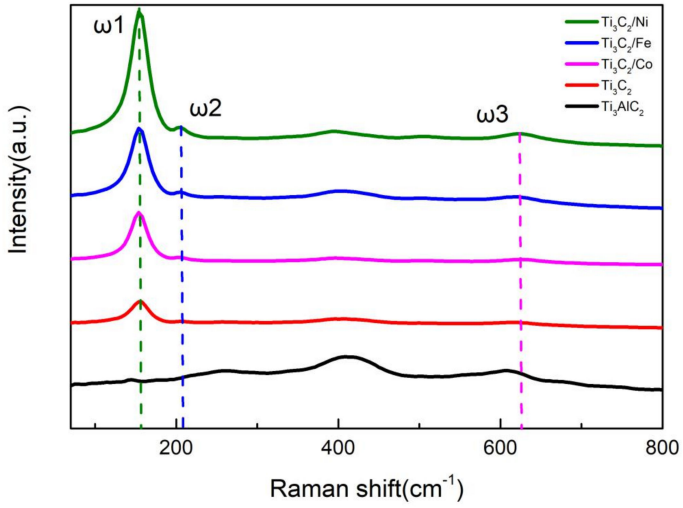

Figure 5. Raman spectra of Ti_3AlC_2, Ti_3C_2, and $Ti_3C_2/Fe^{3+}/Co^{2+}Ni^{2+}$ powders.

For convenience of EMI shielding testing, Ti_3C_2 and Ti_3C_2:$Fe^{3+}/Co^{2+}/Ni^{2+}$ powders are made into thin films through vacuum filtration, and a schematic diagram of a thin film is shown in Figure 6. First, the thicknesses of Ti_3C_2, $Ti_3C_2/Fe^{3+}/Co^{2+}/Ni^{2+}$ films is measured, which have the same thickness, all are 0.05 mm. Then, since electrical conductivity is an important factor in EMI shielding, the electrical conductivity of Ti_3C_2, $Ti_3C_2/Fe^{3+}/Co^{2+}/Ni^{2+}$ films is tested, and the corresponding values are 450, 880, 650, and 600 $Ms{\cdot}cm^{-1}$, as shown in Figure 7. It shows that the electrical conductivity increases when Ti_3C_2 is adsorbed by $Fe^{3+}/Co^{2+}/Ni^{2+}$ ions, because the metal ions adsorption can enhance the conductivity of the materials. The EMI shielding performance of the materials is tested by the coaxial transmission/reflection method. The film is fixed at the connection of the two transmission lines. By transmitting the set electromagnetic wave, the S parameter data of the four materials in the frequency range of 8–18 GHz can be obtained. Using the equivalent S parameter, the transmittance (T), reflectance (R), and absorbance (A) of the tested material can be obtained. The ratio of incident electromagnetic wave power (P_O) and transmitted electromagnetic wave power (P_I) can be calculated, and the EMI SE of the materials can be obtained. The specific formulas are as follows [49–51]:

$$T = 10^{\frac{S_{21}}{10}} \quad (1)$$

$$R = 10^{\frac{S_{11}}{10}} \quad (2)$$

$$A = 1 - R - T \quad (3)$$

$$SE = |S_{21}| = -10\log\left(\frac{P_O}{P_I}\right) \quad (4)$$

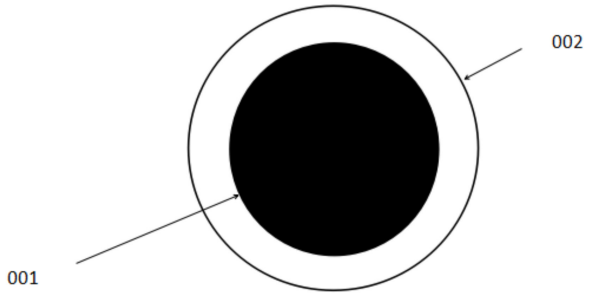

Figure 6. Schematic diagram of a thin film of Ti_3C_2 or Ti_3C_2:Fe^{3+}/Co^{2+}/Ni^{2+} powders obtained through vacuum filtration (001 is a Ti_3C_2/metal ion film, and 002 is a nylon filter membrane).

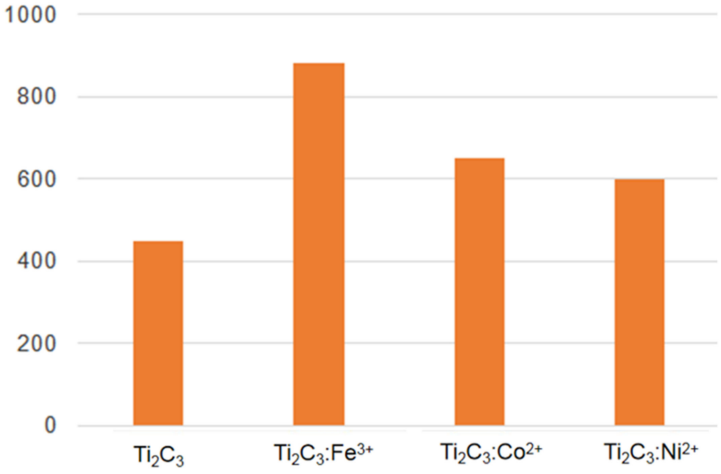

Figure 7. The electrical conductivity of Ti_3C_2, Ti_3C_2/Fe^{3+}/Co^{2+}/Ni^{2+} films.

In our paper, the EMI SEs of Ti_3C_2 and Ti_3C_2/Fe^{3+}/Co^{2+}/Ni^{2+} films are studied in the frequency range of 8–18 GHz, and the EMI SE-frequency curves are shown in Figure 8. We can observe that the EMI SEs are improved to different degrees when Ti_3C_2 is adsorbed by Fe^{3+}/Co^{2+}/Ni^{2+} ions, which is consistent with the electrical conductivity phenomenon. The EMI shielding increased with the increase of the electrical conductivity of Ti_3C_2/Fe^{3+}/Co^{2+}/Ni^{2+} films, and the conductive network attenuated the incident electromagnetic energy through the flow of electrons and internal scattering at the numerous interfaces. Furthermore, the average EMI SEs of the four materials at 8.5–15.5 GHz can be calculated as 3.35, 5.30, 4.51, and 4.32 dB, and the histogram is shown in Figure 9. The most obvious effect is observed for the Ti_3C_2:Fe^{3+} film. As we know, there are many factors that affect EMI SE, such as structural forms, composition, thickness, electrical conductivity, and so on [37]. Table 1 shows the EMI shielding performance of various structural forms based on MXenes.

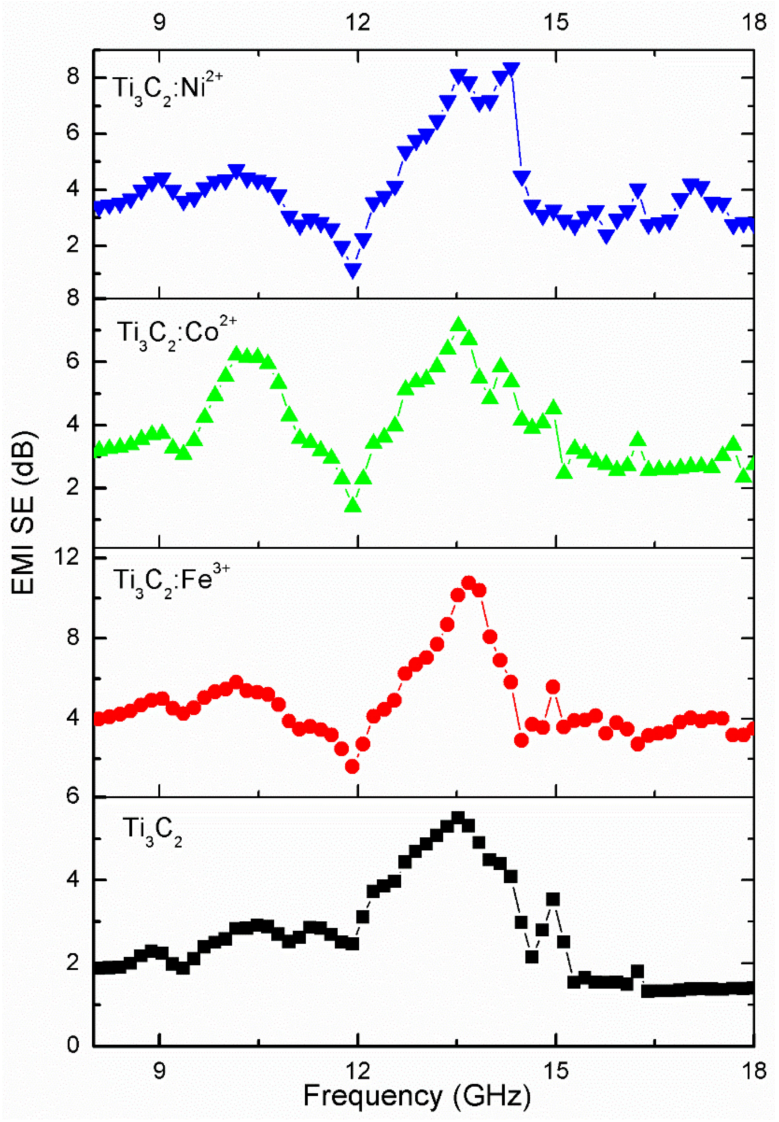

Figure 8. EMI SE-frequency curves of Ti_3C_2, $Ti_3C_2/Fe^{3+}/Co^{2+}/Ni^{2+}$ films from 8–18 GHz.

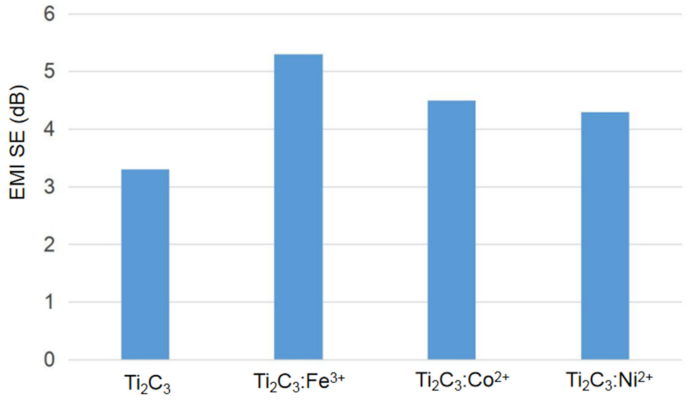

Figure 9. Average shielding effectiveness of Ti_3C_2, $Ti_3C_2/Fe^{3+}/Co^{2+}/Ni^{2+}$ films from 8.5–15.5 GHz.

Table 1. EMI shielding performance of various structural forms based on MXenes.

Structural Forms	Composition	Thickness (mm)	SE (dB)	Ref.
Compact & laminates structures	$Ti_3C_2T_x$	0.045	92	[36]
	$Ti_3C_2T_x$/CNF	0.047	24	[27]
	$Ti_3C_2T_x$/Ni	1.3	33.8	[52]
Layer-by-layer	$Ti_3C_2T_x$/CNT	0.0002	2.9	[53]
	$Ti_3C_2T_x$/PPy	0.45	42	[54]
Porous	$Ti_3C_2T_x$	1	70.6	[55]
	$Ti_3C_2T_x$/PVA	5	33	[56]
Segregated	$Ti_3C_2T_x$/NR	0.25	53.6	[57]

4. Conclusions

In summary, this paper proposes a method for fabricating composites by adsorbing $Fe^{3+}/Co^{2+}/Ni^{2+}$ ions into layered Ti_3C_2. The metal ions adsorption can improve the electrical conductivity in the materials, and the conductive network attenuated the incident electromagnetic energy through the flow of electrons and internal scattering at the numerous interfaces. Therefore, the Ti_3C_2:$Fe^{3+}/Co^{2+}/Ni^{2+}$ composites have a better EMI shielding effectiveness than the pure Ti_3C_2 material. These good EMI shielding materials can potentially be used in communications, electronics, military, and other applications.

Author Contributions: Q.X. designed the project; X.X. and Q.X. analyzed the data; X.X. draft the manuscript. All authors have read and agreed to the published version of the manuscript.

Funding: This research was funded by the Science and Technology Innovation Commission of Shenzhen (JCYJ20190808144015264, GJHZ20200731095809026) and Natural Science Foundation of SZU (No. 860-000002110435).

Institutional Review Board Statement: Not applicable.

Informed Consent Statement: Not applicable.

Data Availability Statement: Data is contained within the article.

Conflicts of Interest: The authors declare no conflict of interest.

References

1. Jalali, M.; Dauterstedt, S.; Michaud, A.; Wuthrich, R. Electromagnetic shielding of polymer-matrix composites with metallic nanoparticles. *Compos. Part B Eng.* **2011**, *42*, 1420–1426. [CrossRef]
2. Naguib, M.; Kurtoglu, M.; Presser, V.; Lu, J.; Niu, J.J.; Heon, M.; Hultman, L.; Gogotsi, Y.; Barsoum, M.W. Two-dimensional nanocrystals produced by exfoliation of Ti_3AlC_2. *Adv. Mater.* **2011**, *23*, 4248–4253. [CrossRef] [PubMed]
3. Huang, W.C.; Zhu, J.; Wang, M.K.; Hu, L.P.; Tang, Y.F.; Shu, Y.Q.; Xie, Z.J.; Zhang, H. Emerging mono-elemental bismuth nanostructures: Controlled synthesis and their versatile applications. *Adv. Funct. Mater.* **2021**, *31*, 2007584. [CrossRef]
4. Song, Q.; Ye, F.; Yin, X.W.; Li, W.; Li, H.J.; Liu, Y.S.; Xie, K.Y.; Li, X.H.; Fu, Q.G.; Cheng, L.F.; et al. Carbon nanotube-multilayered graphene edge plane core-shell hybrid foams for ultrahigh-performance electromagnetic-interference shielding. *Adv. Mater.* **2017**, *29*, 1701583. [CrossRef] [PubMed]
5. Huang, W.C.; Wang, M.K.; Hu, L.P.; Wang, C.; Xie, Z.J.; Zhang, H. Recent advances in semiconducting monoelemental selenium nanostructures for device applications. *Adv. Funct. Mater.* **2020**, *30*, 2003301. [CrossRef]
6. Xiong, D.B.; Li, X.F.; Bai, Z.M.; Lu, S.G. Recent advances in layered $Ti_3C_2T_x$ MXene for electrochemical energy storage. *Small* **2018**, *14*, 1703419. [CrossRef]
7. Liu, J.; Zhang, H.B.; Sun, R.H.; Liu, Y.F.; Liu, Z.S.; Zhou, A.G.; Yu, Z.Z. Hydrophobic, flexible, and lightweight MXene foams for high-performance electromagnetic-interference shielding. *Adv. Mater.* **2017**, *29*, 1702367. [CrossRef]
8. Zhou, Z.H.; Liu, J.Z.; Zhang, X.X.; Tian, D.; Zhan, Z.Y.; Lu, C.H. Ultrathin MXene/calcium alginate aerogel film for high-performance electromagnetic interference shielding. *Adv. Mater. Interfaces* **2019**, *6*, 1802040. [CrossRef]
9. Wang, M.K.; Zhu, J.; Zi, Y.; Wu, Z.G.; Hu, H.G.; Xie, Z.J.; Zhang, Y.; Hu, L.P.; Huang, W.C. Functional two-dimensional black phosphorus nanostructures towards next-generation devices. *J. Mater. Chem. A* **2021**, *9*, 12433–12473. [CrossRef]
10. Das, T.K.; Ghosh, P.; Das, N.C. Preparation, development, outcomes, and application versatility of carbon fiber-based polymer composites: A review. *Adv. Compos. Hybrid Mater.* **2019**, *1*, 1–20. [CrossRef]
11. Bhawal, P.; Ganguly, S.; Das, T.K.; Mondal, S.; Nayak, L.; Das, N.C. A comparative study of physico-mechanical and electrical properties of polymer-carbon nanofiber in wet and melt mixing methods. *Mater. Sci. Eng. B* **2019**, *245*, 95–106. [CrossRef]

12. Mondal, S.; Revindren, R.; Shin, B.; Kim, S.; Lee, H.; Ganguly, S.; Das, N.C.; Nah, C. Electrical conductivity and electromagnetic interference shielding effectiveness of nano-structured carbon assisted poly(methyl methacrylate) nanocomposites. *Polym. Eng. Sci.* **2020**, *60*, 2414–2427. [CrossRef]
13. Ling, J.Q.; Zhai, W.T.; Feng, W.W.; Shen, B.; Zhang, J.F.; Zheng, W.G. Facile preparation of lightweight microcellular polyetherimide/graphene composite foams for electromagnetic interference shielding. *ACS Appl. Mater. Interfaces* **2013**, *5*, 2677–2684. [CrossRef]
14. Ganguly, S.; Ghosh, S.; Das, P.; Das, T.K.; Ghosh, S.K.; Das, N.C. Poly(N-vinylpyrrolidone)-stabilized colloidal graphene-reinforced poly(ethylene-co-methyl acrylate) to mitigate electromagnetic radiation pollution. *Polym. Bull.* **2020**, *77*, 2923–2943. [CrossRef]
15. Li, N.; Huang, Y.; Du, F.; He, H.B.; Lin, X.; Gao, H.J.; Ma, Y.F.; Li, F.F.; Chen, Y.S.; Eklund, P.C. Electromagnetic interference (EMI) shielding of single-walled carbon nanotube epoxy composites. *Nano Lett.* **2006**, *6*, 1141–1145. [CrossRef] [PubMed]
16. Ravindren, R.; Mondal, S.; Bhawal, P.; Ali, S.M.N.; Das, N.C. Superior electromagnetic interference shielding effectiveness and low percolation threshold through the preferential distribution of carbon black in the highly flexible polymer blend composites. *Polym. Compos.* **2019**, *40*, 1404–1418. [CrossRef]
17. Zou, L.H.; Zhang, S.L.; Li, X.P.; Lan, C.T.; Qiu, Y.P.; Ma, Y. Step-by-step strategy for constructing multilayer structured coatings toward high-efficiency electromagnetic interference shielding. *Adv. Mater. Interfaces* **2016**, *3*, 1500476. [CrossRef]
18. Lan, C.T.; Guo, M.; Li, C.L.; Qiu, Y.P.; Ma, Y.; Sun, J.Q. Axial alignment of carbon nanotubes on fibers to enable highly conductive fabrics for electromagnetic interference shielding. *ACS Appl. Mater. Interfaces* **2020**, *12*, 7477–7485. [CrossRef]
19. Shin, B.; Mondal, S.; Lee, M.; Kim, S.; Huh, Y.; Nah, C. Flexible thermoplastic polyurethane-carbon nanotube composites for electromagnetic interference shielding and thermal management. *Chem. Eng. J.* **2021**, *418*, 129282. [CrossRef]
20. Kong, F.Y.; He, X.D.; Liu, Q.Q.; Qi, X.X.; Zhang, Y.T.; Wang, R.G.; Bai, Y.L. Improving the electrochemical properties of MXene Ti_3C_2, multilayer for Li-ion batteries by vacuum calcination. *Electrochim. Acta* **2018**, *265*, 140–150. [CrossRef]
21. Huang, W.C.; Hu, L.P.; Tang, Y.F.; Xie, Z.J.; Zhang, H. Recent advances in functional 2D MXene-based nanostructures for next-generation devices. *Adv. Funct. Mater.* **2020**, *30*, 2005223. [CrossRef]
22. Hantanasirisakul, K.; Zhao, M.Q.; Urbankowski, P.; Halim, J.; Anasori, B.; Kota, S.; Ren, C.E.; Barsoum, M.W.; Gogotsi, Y. Fabrication of $Ti_3C_2T_x$ MXene transparent thin films with tunable optoelectronic properties. *Adv. Electron. Mater.* **2016**, *2*, 1600050. [CrossRef]
23. Ghidiu, M.; Kota, S.; Drozd, V.; Barsoum, M.W. Pressure-induced shear and interlayer expansion in Ti_3C_2 MXene in the presence of water. *Sci. Adv.* **2018**, *4*, eaao65850. [CrossRef]
24. Huang, W.C.; Ma, C.Y.; Li, C.; Zhang, Y.; Hu, L.P.; Chen, T.T.; Tang, Y.F.; Ju, J.F.; Zhang, H. Highly stable MXene (V_2CT_x)-based harmonic pulse generation. *Nanophotonics* **2020**, *9*, 2577–2585. [CrossRef]
25. Peng, C.; Yang, X.F.; Li, Y.H.; Yu, H.; Wang, H.J.; Peng, F. Hybrids of two-dimensional Ti_3C_2 and TiO_2 exposing {001} facets toward enhanced photocatalytic activity. *ACS Appl. Mater. Interfaces* **2016**, *8*, 6051–6060. [CrossRef]
26. Zhang, T.; Pan, L.M.; Tang, H.; Du, F.; Guo, Y.H.; Qiu, T.; Yang, J. Synthesis of two-dimensional $Ti_3C_2T_x$ MXene using HCl + LiF etchant: Enhanced exfoliation and delamination. *J. Alloy. Compd.* **2017**, *695*, 818–826. [CrossRef]
27. Cao, W.T.; Chen, F.F.; Zhu, Y.J.; Zhang, Y.G.; Jiang, Y.Y.; Ma, M.G.; Chen, F. Binary strengthening and toughening of MXene/cellulose nanofiber composite paper with nacre-inspired structure and superior electromagnetic interference shielding properties. *ACS Nano* **2018**, *12*, 4583–4593. [CrossRef]
28. Autere, A.; Jussila, H.; Dai, Y.Y.; Wang, Y.D.; Lipsanen, H.; Sun, Z.P. Nonlinear optics with 2D layered materials. *Adv. Mater.* **2018**, *30*, 1705963. [CrossRef]
29. Lukatskaya, M.R.; Mashtalir, O.; Ren, C.E.; Agnese, Y.D.; Rozier, P.; Taber, P.L. Cation intercalation and high volumetric capacitance of two-dimensional titanium carbide. *Science* **2013**, *341*, 1502–1505. [CrossRef]
30. Srimuk, P.; Halim, J.; Lee, J.; Tao, Q.Z.; Rosen, J.; Presser, V. Two-dimensional molybdenum carbide (MXene) with divacancy ordering for brackish and seawater desalination via cation and anion intercalation. *ACS Sustain. Chem. Eng.* **2018**, *6*, 3739–3747. [CrossRef]
31. Zhang, C.F.; Anasori, B.; Ascaso, A.S.; Park, S.H.; McEvoy, N.; Shmeliov, A.; Duesberg, G.S.; Coleman, J.N.; Gogotsi, Y.; Nicolosi, V. Transparent, flexible, and conductive 2D titanium carbide (MXene) films with high volumetric capacitance. *Adv. Mater.* **2017**, *29*, 1702678. [CrossRef]
32. Zhang, C.F.; Pinilla, S.; McEvoy, N.; Cullen, C.P.; Anasori, B.; Long, E.; Park, S.H.; Ascaso, A.S.; Shmeliov, A.; Krishnan, D.; et al. Oxidation stability of colloidal two-dimensional titanium carbides (MXenes). *Chem. Mater. A Publ. Am. Chem. Soc.* **2017**, *29*, 4848–4856. [CrossRef]
33. Ding, L.; Wei, Y.Y.; Wang, Y.J.; Chen, H.B.; Caro, J.; Wang, H.H. A two-dimensional lamellar membrane: MXene nanosheet stacks. *Angew. Chem.* **2017**, *56*, 1825–1829. [CrossRef]
34. Naguib, M.; Mochalin, V.N.; Barsoum, M.W.; Gogotsi, Y. 25th anniversary article: MXenes: A new family of two-dimensional materials. *Adv. Mater.* **2014**, *26*, 992–1005. [CrossRef]
35. Yun, T.; Kim, H.; Iqbal, A.; Cho, Y.S.; Lee, G.S.; Kim, M.K.; Kim, S.J.; Kim, D.; Gogotsi, Y.; Kim, S.O.; et al. Electromagnetic shielding of monolayer MXene assemblies. *Adv. Mater.* **2020**, *32*, 1906769. [CrossRef] [PubMed]
36. Shahzad, F.; Alhabeb, M.; Hatter, C.B.; Anasori, B.; Hong, S.M.; Koo, C.M.; Gogotsi, Y. Electromagnetic interference shielding with 2D transition metal carbides (MXenes). *Science* **2016**, *353*, 1137–1140. [CrossRef] [PubMed]
37. Iqbal, A.; Sambyal, P.; Koo, C.M. 2D MXenes for electromagnetic shielding: A review. *Adv. Funct. Mater.* **2020**, *30*, 2000883. [CrossRef]
38. Hu, T.; Wang, J.M.; Zhang, H.; Li, Z.J.; Hu, M.M.; Wang, X.H. Vibrational properties of Ti_3C_2 and $Ti_3C_2T_2$ (T = O, F, OH) monosheets by first-principles calculations: A comparative study. *Phys. Chem. Chem. Phys.* **2015**, *15*, 1–7.

39. Das, P.; Ganguly, S.; Saha, A.; Noked, M.; Margel, S.; Gedanken, A. Carbon-dots-initiated photopolymerization: An in situ synthetic approach for MXene/poly(norepinephrine)/copper hybrid and its application for mitigating water pollution. *ACS Appl. Mater. Interfaces* **2021**, *13*, 31038–31050. [CrossRef] [PubMed]
40. Chen, X.; Sun, X.K.; Xu, W.; Pan, G.C. Ratiometric photoluminescence sensing based on Ti_3C_2 MXene quantum dots for the intracellular pH sensor. *Nanoscale* **2018**, *3*, 1–8.
41. Xue, Y.H.; Zhang, Q.; Wang, W.J.; Cao, H.; Yang, Q.H.; Fu, L. Opening two-dimensional materials for energy conversion and storage: A concept. *Adv. Energy Mater.* **2017**, *7*, 1602684. [CrossRef]
42. Yuan, H.T.; Wang, H.T.; Cui, Y. Two-dimensional layered chalcogenides: From rational synthesis to property control via orbital occupation and electron filling. *Acc. Chem. Res.* **2015**, *48*, 81–90. [CrossRef] [PubMed]
43. Han, M.K.; Yin, X.W.; Wu, H.; Hou, Z.X.; Song, C.Q.; Li, X.L.; Zhang, L.T.; Cheng, L.F. Ti_3C_2 MXenes with modified surface for high-performance electromagnetic absorption and shielding in the X-Band. *ACS Appl. Mater. Interfaces* **2016**, *8*, 21011–21019. [CrossRef]
44. Li, H.; Lian, P.C.; Lu, Q.J.; Chen, J.C.; Hou, R.R.; Mei, Y. Excellent air and water stability of two-dimensional black phosphorene/MXene heterostructure. *Mater. Res. Express* **2019**, *6*, 065504. [CrossRef]
45. Zhang, L.X.; Su, W.T.; Huang, Y.W.; Li, H.; Fu, L.; Song, K.X.; Huang, X.W.; Yu, J.H.; Lin, C.T. In situ high-pressure X-ray diffraction and raman spectroscopy study of $Ti_3C_2T_x$ MXene. *Nanoscale Res. Lett.* **2018**, *13*, 343. [CrossRef]
46. Hu, T.; Hu, M.M.; Li, Z.J.; Zhang, H.; Zhang, C.; Wang, J.M.; Wang, X.H. Covalency-dependent vibrational dynamics in two-dimensional titanium carbides. *J. Phys. Chem. A* **2015**, *119*, 12977–12984. [CrossRef]
47. Jiang, X.T.; Liu, S.X.; Liang, W.Y.; Luo, S.J.; He, Z.L.; Ge, Y.Q.; Wang, H.D.; Cao, R.; Zhang, F.; Wen, Q.; et al. Broadband nonlinear photonics in few-layer MXene $Ti_3C_2T_x$ (T = F, O, or OH). *Laser Photonics Rev.* **2018**, *12*, 1700229. [CrossRef]
48. Shi, C.Y.; Beidaghi, M.; Naguib, M.; Mashtalir, O.; Gogotsi, Y.; Billinge, S.J.L. Structure of nanocrystalline Ti_3C_2 MXene using atomic pair distribution function. *Phys. Rev. Lett.* **2014**, *112*, 125501. [CrossRef]
49. Bhawal, P.; Ganguly, S.; Das, T.K.; Mondal, S.; Das, N.C. Mechanically robust conductive carbon clusters confined ethylene methyl acrylate-based flexible composites for superior shielding effectiveness. *Polym. Adv. Technol.* **2018**, *29*, 95–110. [CrossRef]
50. Mondal, S.; Ganguly, S.; Das, P.; Bhawal, P.; Das, T.K.; Nayak, L.; Khastgir, D.; Das, N.C. High-performance carbon nanofiber coated cellulose filter paper for electromagnetic interference shielding. *Cellulose* **2017**, *24*, 5117–5131. [CrossRef]
51. Zou, L.H.; Lan, C.T.; Li, X.P.; Zhang, S.L. Superhydrophobization of cotton fabric with multiwalled carbon nanotubes for durable electromagnetic interference shielding. *Fibers Polym.* **2015**, *16*, 2158–2164. [CrossRef]
52. Liang, L.Y.; Han, G.J.; Li, Y.; Zhao, B.; Zhou, B.; Feng, Y.Z.; Ma, J.M.; Wang, Y.M.; Zhang, R.; Liu, C.T. Promising $Ti_3C_2T_x$ MXene/Ni chain hybrid with excellent electromagnetic wave absorption and shielding capacity. *ACS Appl. Mater. Interfaces* **2019**, *11*, 25399–25409. [CrossRef] [PubMed]
53. Weng, G.M.; Li, J.; Alhabeb, M.; Karpovich, C.; Wang, H.; Lipton, J.; Maleski, K.; Kong, J.; Shaulsky, E.; Elimelech, M.; et al. Layer-by-layer assembly of cross-functional semi-transparent MXene-carbon nanotubes composite films for next-generation electromagnetic interference shielding. *Adv. Funct. Mater.* **2018**, *28*, 1803360. [CrossRef]
54. Wang, Q.W.; Zhang, H.B.; Liu, J.; Zhao, S.; Xie, X.; Liu, L.; Yang, R.; Koratkar, N.; Yu, Z.Z. Multifunctional and water-resistant MXene-decorated polyester textiles with outstanding electromagnetic interference shielding and joule heating performances an efficient and scalable dip-coating multifunctional textiles. *Adv. Funct. Mater.* **2019**, *29*, 1806819. [CrossRef]
55. Han, M.; Yin, X.; Hantanasirisakul, K.; Li, X.; Iqbal, A.; Hatter, C.B.; Anasori, B.; Koo, C.M.; Torita, T.; Soda, Y.; et al. Anisotroic MXene aerogels with a mechanically tunable ratio of electromagnetic wave reflection to absorption. *Adv. Opt. Mater.* **2019**, *7*, 1900267. [CrossRef]
56. Xu, H.L.; Yin, X.W.; Li, X.L.; Li, M.H.; Liang, S.; Zhang, L.T.; Cheng, L.F. Lightweight Ti2CTx MXene/poly(vinyl alcohol) composite foams for electromagnetic wave shielding with absorption-dominated feature. *ACS Appl. Mater. Interfaces* **2019**, *11*, 10198–10207. [CrossRef]
57. Luo, J.Q.; Zhao, S.; Zhang, H.B.; Deng, Z.; Li, L.; Yu, Z.Z. Flexible, stretchable and electrically conductive MXene/natural rubber nanocomposite films for efficient electromagnetic interference shielding. *Compos. Sci. Technol.* **2019**, *182*, 107754. [CrossRef]